Front. Earth Sci. 2022, 16(4): 989−1004
https://doi.org/10.1007/s11707-021-0960-3

RESEARCH ARTICLE

Cenozoic potassic volcanic rocks from the Keluo and Wudalianchi volcanic districts, northeast China: origin from the new sub-continental lithospheric mantle (SCLM) metasomatized by potassium-rich fluids from delaminated lower crust

Fanchao MENG (✉)[1,2,3], Yulu TIAN[1], Yaoqi ZHOU[1,2,3], Jiaqi LIU[4], Gengchao ZUO[1], Qing DU[1]

1 School of Geosciences, China University of Petroleum (East China), Qingdao 266580, China
2 Pilot National Laboratory for Marine Science and Technology (Qingdao), Qingdao 266061, China
3 Shandong Provincial Key Laboratory of Deep Oil and Gas, China University of Petroleum (East China), Qingdao 266580, China
4 Institute of Geology, Chinese Academy of Geological Sciences, Beijing 100037, China

Abstract A series of Cenozoic potassium-rich volcanic rocks developed in the Xiaoguli-Keluo-Wudalianchi-Erkeshan districts, northeast China. The source region and potassium-rich mechanism of the potassic rocks remain highly disputed. In this paper, the major elements, trace elements, and Sr-Nd-Pb isotopes of the volcanic rocks in Keluo (KL) and Wudalianchi (WDLC) volcanic districts were analyzed systematically. The results show that the volcanic rocks are characterized by high K_2O (4.36wt.% −6.13wt.%), remarkable enrichment in LREEs and LILEs, as well as the strong fractionation of HREEs. The isotopic characteristics with high $^{87}Sr/^{86}Sr$ (0.704990–0.705272), low $^{143}Nd/^{144}Nd$ (0.512306–0.512417), low $^{206}Pb/^{204}Pb$ (16.546–17.135) and $^{207}Pb/^{204}Pb$ (15.002–15.783) of the volcanic rocks suggest the involvement of EM-I-type mantle. On the basis of the geochemical characteristics, the potassium-rich volcanic magma originated from the new SCLM forming after delamination of the ancient SCLM, with metasomatism of the potassium-rich fluids released from the ancient lower crust during the Late Mesozoic. The proposed genetic model assumes the source which represented by a phlogopite-bearing garnet peridotite (with modal garnet in the range of 2%–10%) experienced very low degrees (i.e., ~0.5) of partial melting. During Cenozoic, the lithosphere in northeast China was affected by the extension and decompression of continental rift, and the metasomatized SCLM underwent low degree partial melting, resulting in the formation of potassium-rich primitive basaltic magma.

Keywords northeast China, Keluo-Wudalianchi volcanic districts, Cenozoic potassic volcanic rocks, petrogenesis, sub-continental lithospheric mantle

Received August 4, 2021; accepted November 29, 2021

E-mail: mengfc@upc.edu.cn

1 Introduction

Potassium-rich igneous rocks are characterized by high K_2O contents (K_2O > 3wt.%) and K_2O/Na_2O ratios (molar K_2O/Na_2O > 1), usually accompanied by other geochemical features such as high MgO, Ni, and Cr contents, indicating that they have undergone relatively limited differentiation (Foley and Peccerillo, 1992). Potassium-rich rocks generally develop in various tectonic settings, including subduction-related environments, such as island arcs (e.g., Indonesia) and post-collisional settings (e.g., Italy and southern Tibet), and intraplate, such as active rifting (e.g., Toro-Ankole Province of the East African Rift) and hotspot regions (e.g., Western Australia, Gaussberg, and Leucite Hills) (Foley and Peccerillo, 1992; Zhang et al., 1995; Murphy et al., 2002; Zou et al., 2003; Davies et al., 2006; Chen et al., 2007; Prelevic and Foley, 2007; Avanzinelli et al., 2007; Chu et al., 2013; Kuritani et al., 2013; Sun et al., 2014; Sun et al., 2015). With the difference of tectonic environment, potassic rocks have distinct petrogenetic mechanisms (Xu et al., 2012; Chu et al., 2013; Kuritani et al., 2013; Tian et al., 2016; Wang et al., 2017; Fan et al., 2021). Sub-continental lithospheric mantle (SCLM) and recycled crustal materials are generally

considered as two source endmembers of the potassium-rich volcanic rocks from intraplate region or plate margin. However, the mechanism responsible for recycling of crustal materials into the mantle source is still of considerable debate: lithospheric delamination or plate subduction?

Cenozoic intraplate volcanoes are widely distributed in northeast China, with more than 590 Cenozoic volcanoes (Liu et al., 2001; Meng et al., 2018), making northeast China one of the best places to study the genesis of intraplate volcanoes. Most Cenozoic volcanic rocks in northeast China are sodic volcanic rocks, with the exception of the potassic volcanic rocks in Xiaoguli, Keluo, Wudalianchi, and Erkeshan regions characterized by high K, light rare earth elements (LREEs), and large ion lithophile elements (LILEs). (Fig. 1) (Zhang et al., 1995; Zou et al., 2003; Chu et al., 2013; Zhao et al., 2014). Nowadays the sources of these potassic magmas are in dispute, with the main points as follows: 1) the continental lithospheric mantle (Zhang et al., 1995; Chen et al., 2007); 2) the asthenosphere mantle containing delaminated continental lithosphere mantle fragment (Choi et al., 2006); 3) mantle transition zone metasomatized by potassium-rich sediments (Kuritani et al., 2013).

The dominant viewpoint is that the potassium-rich volcanic rocks come directly from the metasomatized lithospheric mantle. However, various sources of metasomatic materials have been proposed, including the ancient subducted sediments in the mantle transition zone (Sun et al., 2015), delamination of the ancient lower crust (Chu et al., 2013), and some uncertain enriched substances in the asthenosphere (Zhang et al., 1995; Zou et al., 2003; Wang et al., 2017).

Recently, Fan et al. (2021) presented a high-resolution, three-dimensional (3-D) crust and upper-mantle S-wave velocity model of northeast China by combining ambient noise and earthquake two-plane wave tomography based on unprecedented regional dense seismic arrays. The model shows that there are imprints of the interaction between asthenospheric low-degree melts and the overlying subcontinental lithospheric mantle (Fan et al., 2021). However, it is not feasible to determine the melt source only by geophysics. In view of this, this paper reports new geochemical data of volcanic rocks in the less studied districts of Keluo and Wudalianchi, such as Nanshan, Dayishan, Huoshaoshan, and Bijiashan. Combining the published geochemical and geophysical data of the potassium-rich volcanic rocks, new insights into the genesis of the potassium-rich volcanic rocks are put forward.

2 Geological background

The Xiaoguli-Keluo-Wudalianchi-Erkeshan districts (northeast China) at the eastern end of the Central Asian orogenic belt (Jahn et al., 2000) are located at the junction of the northern margin of the North China Craton, the southeastern margin of the Siberian Plate and the subduction zone of the West Pacific Plate (Fig. 1(a)) (Ren et al., 2002; Zhang et al., 2006; Zhou et al., 2009). Since the Paleozoic Era, this area has experienced the tectonic evolution of the Paleo-Asian Ocean, the Mongolian-Okhotsk Sea, and circum-Pacific systems (Zhao et al., 1994). During the Paleozoic Era, the Ergun-Xing'an, Songneng-Zhangguangcai, and Jiamusi microcontinental blocks converged and joined with the North China Craton and Siberian Craton (Li, 2006; Zhang et al., 2006). During the Mesozoic, the tectonic setting in this area transited from the Mongol-Okhotsk tectonic system to the Pacific tectonic system accompanied by multi-phased tectonic-magmatic processes (Wu et al., 2000; Xu et al., 2013; Meng et al., 2014). During the Cenozoic, northeast China was in an extensional tectonic setting with the formation of continental rift, and with diffuse basaltic magmatism marking a clear compositional change with respect to the previous Mesozoic cycle dominated by acid rocks (Liu et al., 2001). Cenozoic volcanic rocks are widespread in northeast China, covering an area of approximately 50000 km^2 (Fig. 1(a)) (Liu, 1999; Liu et al., 2001).

There is a volcanic belt with a total length of more than 300 km and an area of more than 14000 km^2 in the narrow zone between the Songliao Basin and the Great Xing'an Range in northeast China. It is one of the best preserved Cenozoic volcanic districts in China, including Xiaoguli, Menlu, Keluo, Wudalianchi, and Erkeshan volcanic districts from north to south (Fig. 1(b)) (Fan et al., 1999; Li et al., 2012). Over 80% volcanic rocks are distributed in Keluo and Wudalianchi volcanic districts (Zhao et al., 2014), and there are a large amount of mantle xenoliths in the volcanic rocks in that area (Zhang et al., 2000; Zhang et al., 2011). The Keluo volcanic district consists of nearly 40 small volcanic cones, including the Nanshan, Dayishan, Heshan, and Gushan, which cover an area of approximately 350 km^2 (Fig. 1(c)). The younger basaltic pumice and volcanic cinder fell on alluvial gravel beds, while the older basalt was overlaid on the mountain top with a height of 450–600 m as a form of high platform and cap (Liu, 1999).The Keluo volcanic group erupted in two periods. The early eruption occurred during Early Pliocene to Early Pleistocene (4.59–1.51 Ma) and the late eruption occurred during Middle Pleistocene (1.34–0.133 Ma) (Zhao et al., 2014). The Wudalianchi volcanic district located on the northern bank of the Nemuoer River is the product of multi-phased magmatic activities. It consists of 11 shield volcanoes and 15 volcanic cones (Xu, 1997), covering an area of 800 km^2 (Fig. 1(d)). During the early stage, lava flows prevailed, forming a low shield volcano or lava mound. However, during the late stages, the volcanic cone was composed of lava flow and weakly erupted debris (Fan et al., 1999). The volcanic activity of Wudalianchi lasted from Early Pleistocene to Holocene (Liu et al., 2001; Zhao et al., 2014).

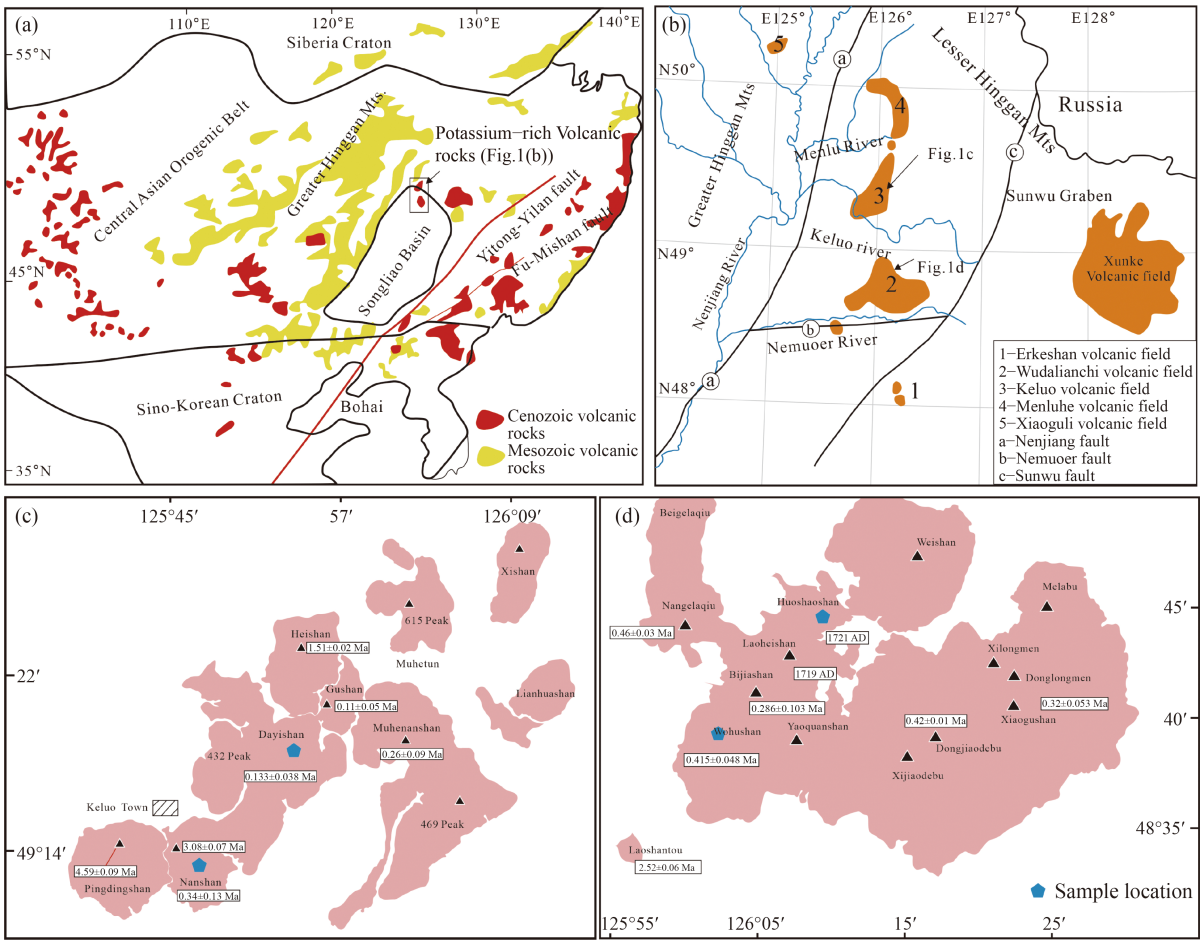

Fig. 1 (a) Geological sketch of northeast China (after Ren et al., 2002); (b) the investigated Cenozoic potassium-rich volcanic districts (after Zhao et al., 2014); (c) Geological sketch maps of Keluo and (d) Wudalianchi volcanic districts (after Zhao et al., 2014).

The Laoheishan and Huoshaoshan volcanoes erupted from 1719 to 1721.

3 Samples and petrography

The samples of the Keluo volcanic group were collected from Dayizishan and Nanshan volcanic cones, which were mainly composed of basanite and melanocratic leucite-basanite. The samples of Wudalianchi were from Bijiashan and Huoshaoshan volcanic cones (Figs. 2(a) –2(c)), consisting of leucite basalt, murambite, and trachybasalt. The samples of volcanic rocks are mainly porphyritic, with phenocrysts accounting for about 4%–10%, and matrix accounting for 90%–96%. The phenocrysts are mainly composed of olivine and clinopyroxene. The olivine is automorphic hexagonal or granular crystal, with the size of about 0.1–0.6 mm. Clinopyroxene occurs as 0.1–0.8 mm automorphic or hypautomorphic crystal. The matrix is mostly cryptocrystalline and a small amount is microcrystalline. Alteration can be seen in some phenocrysts with embay-like erosion edges (Figs. 2(d) –2(f)).

4 Analytical methods

All the samples were analyzed at the Testing Center of Institute of Geology, Ministry of Nuclear Industry in Beijing (TCIGNI). Whole-rock major element contents were determined on fused glass disks by X-ray fluorescence (XRF) using an XRF-PW2404 sequential spectrometer. Sample powders (0.6 g) were fused with $Li_2B_4O_7$ (6 g) in an automatic bead fusion furnace at 1100°C for 10 min. Loss on ignition was determined by igniting 2 g whole-rock powder at 1100°C for 10 h. The analytical precision was better than 2%–3% relative. Trace element contents (including REE, Rare Earth Elements) were analyzed by inductively coupled plasma mass spectrometry (ICP-MS) at TCIGNI using a FINNIGAN MAT I element system. Whole-rock powders (40 mg) were weighed and dissolved in distilled 1 mL HF and 0.5 mL HNO_3 (HNO_3: H_2O = 1:1, in volume ratio) in 7 mL Savillex Teflon screw-cap capsules and then were ultrasonically stirred for 15 min. The solutions were subsequently dried at 150°C and the residue was digested with the same acid solution. Then, the solutions were heated at 170°C for 10 days, dried and

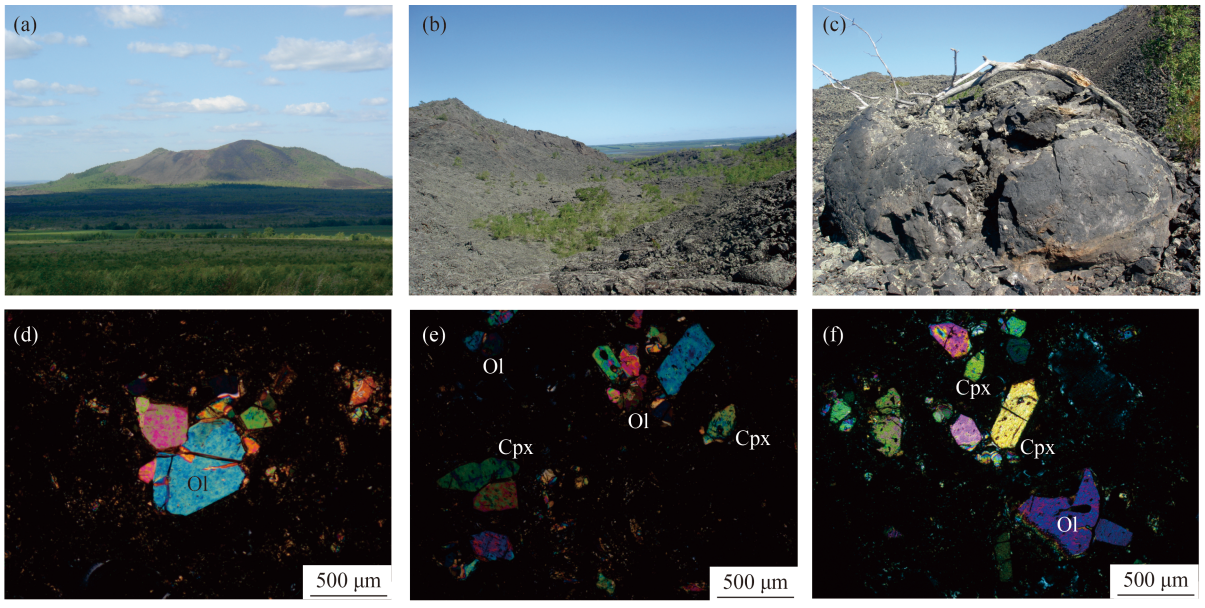

Fig. 2 Photos of outcrops from the Bijiashan (a) and Huoshaoshan (b–c) volcanic cones in Wudalianchi, optical microscope images (d–f) of the Cenozoic volcanic rocks in Wudalianchi in northeast China. Ol, olivine; Cpx, clinopyroxene.

redissolved in 2 mL HNO_3 (HNO_3:H_2O = 1:1, in volume ratio). The solutions were heated at 150°C for 5 h and then evaporated, dried, and redissolved in 2 mL HNO_3 at 150°C for 5 h to ensure that the samples were completely dissolved. 1 mL 500 ppb In was added as an internal standard. Finally, the solutions were diluted in 1% HNO_3 to 50 mL. An international standard (GRS1) was subjected to the same procedure in order to monitor the analytical reproducibility. The analytical precision was better than 5% and 10% relative for the elements with contents larger than 10×10^{-6} and less than 10×10^{-6}, respectively.

For Rb-Sr isotope analyses, sample powders (0.1 g) were spiked with mixed isotope tracers (^{87}Rb-^{84}Sr for Rb-Sr isotope analyses), then dissolved with a mixed acid (HF + HNO_3 + $HClO_4$) in Teflon capsules for 24 h. Subsequently, the solutions were evaporated to dryness and the residue was dissolved in 6 mol/L HCl. The solutions were heated to evaporation, dried, and redissolved in 0.5 mol/L HCl. Then, the solutions were centrifugated and the clear liquid was poured into AG50W × 8 (H^+) cationic ion-exchange resin columns. The Sr fractions were separated using 2.5 mol/L HCl, dried and dissolved in HNO_3 to give solutions for analysis by mass spectrometry. For Sm-Nd isotope analyses, the procedure was as the same as Rb-Sr before eluviation. Sm and Nd were separated from the other REE fractions in solution using 4 mol/L HCL, and Sm and Nd were separated using P_5O_7 extraction and eluviation resin. The collected Nd fractions were then dissolved in HNO_3 to give solutions for analysis by mass spectrometry. The whole procedure blank was less than 0.2 ng for Rb-Sr isotopic analysis and 0.05 ng for Sm-Nd isotopic analysis. Analytical errors for Sr and Nd isotopic ratios are given as 2σ. For Pb isotope measurements, Pb was separated from the silicate matrix and purified using AG1 × 8 anionic ion-exchange columns with dilute HBr as eluant. The whole procedure blank was less than 1 ng.

Sr-Nd-Pb isotope analyses were performed on ISOPROBE-T mass spectrometer. The mass fractionation corrections for Sr and Nd isotopic ratios were based on $^{86}Sr/^{88}Sr$ = 0.1194 and $^{146}Nd/^{144}Nd$ = 0.7219, respectively. The international standard NBS987 gave $^{87}Sr/^{86}Sr$ = 0.710250 ± 7. The JMC standard yielded $^{143}Nd/^{144}Nd$ = 0.512109 ± 3. During the period of Pb isotope analysis repeated analyses of the international standard NBS981 yielded $^{204}Pb/^{206}Pb$ = 0.0591107±2, $^{207}Pb/^{206}Pb$ = 0.914338±7 and $^{208}Pb/^{206}Pb$ = 2.164940±15.

5 Results

5.1 Major elements

The major element results of the volcanic rocks from the KL and WDLC volcanic districts are shown in Table 1. The analyzed samples are rich in alkalis and belong to the group of potassic rocks (Fig. 3(a); i.e., K_2O/Na_2O > 1; Foley and Peccerillo, 1992), with $K_2O + Na_2O$ = 7.92wt.% –10.06wt.%, K_2O = 4.36wt.%–6.13wt.%, K_2O/Na_2O = 1.18–1.59, MgO = 4.24wt.%–7.62wt.%, CaO = 5.34wt.% –7.60wt.%, Al_2O_3 = 13.27wt.%–14.36wt.% and SiO_2 = 49.63wt.%–53.23wt.%. In the TAS classification diagram (Fig. 3(b)), the KL and WDLC volcanic rocks fall in the fields for basaltic trachyandesite, trachyandesite, phonolitic tephrite, tephriphonolite, and tephrite/basanite, dominated by phonolitic tephrite, in accordance with the data from available literature (Fan and Hooper, 1991; Zhang et al., 1991; Zhang et al., 1995; Zou et al., 2003; Chu

Table 1 Major elements (wt.%) and trace elements ($\times 10^{-6}$) contents for the investigated volcanic rocks from the Keluo and Wudalianchi volcanic districts

Sample number	Wudalianchi				Keluo						
	WDLC-1	WDLC-2	WDLC-3	WDLC-4	KL-1	KL-2	KL-3	KL-4	KL-5	KL-6	KL-7
SiO_2	50.14	50.48	49.63	51.82	52.52	51.96	52.46	53.23	53.12	53.20	53.19
TiO_2	2.30	2.30	2.60	2.33	2.35	2.42	2.39	2.71	2.74	2.82	2.81
Al_2O_3	13.27	13.33	13.42	13.86	13.98	14.04	14.16	14.35	14.36	14.35	14.33
$Fe_2O_3^T$	9.69	9.65	9.83	9.01	8.97	9.06	8.67	8.32	8.26	8.63	8.53
MnO	0.131	0.13	0.124	0.116	0.107	0.11	0.11	0.10	0.10	0.101	0.1
MgO	7.62	7.54	7.43	7.08	6.08	5.92	5.88	4.38	4.31	4.25	4.24
CaO	7.60	7.39	7.15	6.70	6.30	6.30	6.17	5.34	5.39	5.46	5.44
Na_2O	3.70	3.69	3.52	3.45	3.55	3.73	3.93	4.11	3.94	3.86	3.95
K_2O	4.36	4.44	4.71	4.47	4.83	5.05	4.93	5.95	5.91	6.13	6.07
P_2O_5	0.988	0.948	0.993	0.901	0.907	0.926	0.93	1.09	1.07	1.09	1.1
LOI	0.10	0.00	0.55	0.16	0.28	0.37	−0.16	0.06	0.22	0.01	0.13
Total	99.90	99.90	99.96	99.90	99.87	99.89	99.47	99.64	99.42	99.90	99.89
La	97.3	94.9	84.4	79.2	82.8	80.8	82.6	95.6	102	103	105
Ce	174	171	151	143	150	147	146	168	178	185	188
Pr	20.2	20	17.3	17.2	17.5	17	16.9	19.9	20.6	21.4	21.7
Nd	77.5	76.5	66.7	64.7	68	66.2	68.1	77.6	78.2	81	79.5
Sm	12.9	12.8	10.9	11.2	11.3	11	10.6	12.2	12.3	13.3	12.9
Eu	3.81	3.8	3.31	3.39	3.34	3.27	3.25	3.57	3.64	3.88	3.78
Gd	10.3	10.3	8.96	9.1	9	8.7	8.87	9.5	9.83	10.3	10
Tb	1.39	1.37	1.2	1.22	1.19	1.15	1.21	1.31	1.32	1.35	1.31
Dy	6.64	6.59	5.84	5.74	5.66	5.41	5.42	5.77	5.71	6.28	6.19
Ho	1.02	1.01	0.89	0.884	0.854	0.824	0.755	0.808	0.856	0.945	0.929
Er	2.6	2.6	2.34	2.41	2.2	2.11	1.91	2.1	2.09	2.37	2.35
Tm	0.299	0.303	0.27	0.292	0.247	0.236	0.213	0.213	0.214	0.265	0.259
Yb	1.65	1.63	1.53	1.65	1.39	1.32	1.39	1.37	1.43	1.47	1.4
Lu	0.218	0.218	0.206	0.225	0.177	0.168	0.182	0.163	0.163	0.18	0.175
Sc	15.3	15.8	15.5	14.7	14.2	13.5	9.55	6.99	6.97	11.6	11.6
V	155	160	163	152	148	146	146	126	119	137	135
Cr	310	334	225	270	247	215	191	101	79.3	149	138
Co	39.3	40.5	38.9	38.7	36.3	35.6	37.3	29.7	30.1	30.2	29.6
Ni	169	168	148	163	111	101	106	58.5	60.5	59.8	58.6
Cu	42.7	42.3	38.5	53.5	33	32.1	40.1	34.3	32.7	34.2	39.5
Zn	131	140	126	129	132	132	137	126	149	142	144
Ga	20.9	22.2	21.8	22.8	25.3	24.3	25.8	25.3	26.9	26.2	26.4
Rb	82.4	86.8	95.7	106	97.6	97.5	102	118	122	120	120
Sr	1563	1550	1361	1408	1296	1326	1158	1348	1443	1618	1588
Y	25.3	25.4	23.2	23.6	21.6	20.8	20.9	21.6	22.5	23.7	23.4
Zr	753	785	787	798	867	826	–	–	–	1183	1170
Nb	61.3	63	65.4	56.1	59.3	57.4	57.1	70.6	74.9	77.2	76.7
Ba	1765	1797	1863	1773	1749	1771	1657	1828	1952	2149	2155
Hf	15.9	16.7	17	17.2	18.4	17.7	–	–	–	24.9	24.8
Ta	3.15	3.27	3.65	3.23	3.18	3.09	3.26	4.09	4.29	4.04	4.04

(*Continued*)

Sample number	Wudalianchi				Keluo						
	WDLC-1	WDLC-2	WDLC-3	WDLC-4	KL-1	KL-2	KL-3	KL-4	KL-5	KL-6	KL-7
Pb	10.9	13.1	10.9	11.2	12.9	9.76	13	16.9	17.9	16.3	16.5
Th	7.32	7.57	7.47	6.56	7.34	6.92	7.17	8.28	8.96	8.97	8.85
U	1.54	1.65	1.54	1.46	1.55	1.48	1.49	1.82	1.98	2.01	1.98
Nb/U	39.81	38.18	42.47	38.42	38.26	38.78	38.32	38.79	37.83	38.41	38.74
Ce/Pb	15.96	13.05	13.85	12.77	11.63	15.06	11.23	9.94	9.94	11.35	11.39

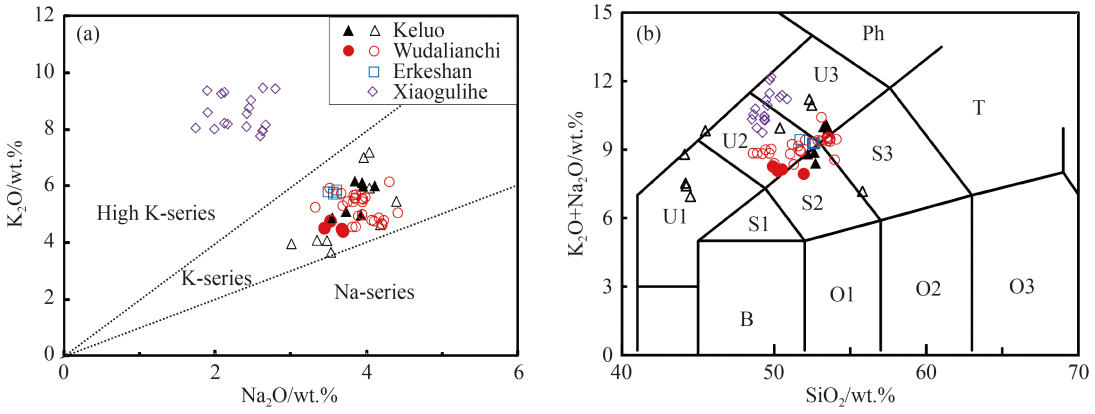

Fig. 3 K_2O-Na_2O ((a), after Foley and Peccerillo, 1992) and TAS ((b), after Le Bas et al., 1986) diagrams for the volcanic rocks from the Keluo and Wudalianchi volcanic districts. B = basalt; Ph = phonolite; *T* = trachyte; O1 = basaltic andesite; O2 = andesite; O3 = dacite; S1 = trachybasalt; S2 = basaltic trachyandesite; S3 = trachyandesite; U1 = tephrite/basanite; U2 = phonotephrite; U3 = tephriphonolite.

et al., 2013). In Harker-type diagrams (Fig. 4), the KL and WDLC volcanic rocks (as well those from the neighboring Erkeshan district) show decreasing $Fe_2O_3^T$ and CaO and increasing Al_2O_3, TiO_2, SiO_2 and K_2O with increasing degree of rock evolution (i.e., decreasing MgO contents). The contents of major element oxides in different regions are not exactly the same. For example, the volcanic rocks in WDLC have higher MgO, CaO, and $Fe_2O_3^T$ contents, lower Al_2O_3, TiO_2, K_2O, and SiO_2 contents, while those in KL have higher Al_2O_3, TiO_2, K_2O, and SiO_2 contents, lower MgO, CaO, and $Fe_2O_3^T$ contents, which is consistent with the results of available studies. However, on the whole, the data points in the KL and WDLC districts are relatively coherent in the Harker-type diagrams (Fig. 4), indicating the source of magma is unified.

Filled and open symbols represent, respectively, data from this study and the available literature (Fan and Hooper, 1991; Zhang et al., 1991; Zhang et al., 1995; Zou et al., 2003; Chu et al., 2013).

5.2 Trace elements

Trace element contents are presented in Table 1. The rocks from the KL and WDLC volcanic districts are rich in REEs (such as La, Ce, Pr, and Nd) and LILEs (such as Rb, Ba, and K). The contents of REEs are 340.21 ‰–433.49 ‰. The chondrite-normalized diagram of REEs (Fig. 5(a)) reveals a right-leaning pattern. The LREEs are rich, with $(La/Yb)_N$ of 34.43–53.80. The fractionation of HREEs (Heavy Rare Earth Elements) is obvious, with average $(Sm/Yb)_N$ ranging from 7.5 to 10.2. There is no Eu negative anomaly. δEu (= Eu/Eu*) is 0.98–1.00, with an average of 0.98.

The volcanic rocks in WDLC have high Ba (1657×10^{-6}–2155×10^{-6}), Sr (1158×10^{-6}–1618×10^{-6}) and Ni (58.5×10^{-6}–169×10^{-6}) contents, but low Th (6.56×10^{-6}–8.97×10^{-6}), U (1.46×10^{-6}–2.01×10^{-6}), and Ta (3.09×10^{-6}–4.29×10^{-6}) contents. Different samples have slightly different Zr and Hf contents. Nanshan in KL has lower Zr (753×10^{-6}–867×10^{-6}) and Hf (15.9×10^{-6}–18.4×10^{-6}), while Dayishan has higher Zr (1176.5×10^{-6}) and Hf (24.85×10^{-6}). Primitive mantle-normalized diagram (Fig. 5(b)) shows that the samples are enriched in LILEs, with evident peaks at Ba, K, Pb, Zr, and Hf. U, Th, Nb, and Ta show slightly negative anomaly. Ce/Pb ranges between 9.94 and 15.96, significantly lower compared with ocean island basalt values (OIB = 25±5, Hofmann, 1986). La/Nb ranges between 1.29 and 1.59 and Ba/Nb between 25.89 and 31.60. Ni, Cr, and MgO have a positive correlation (Fig. 4).

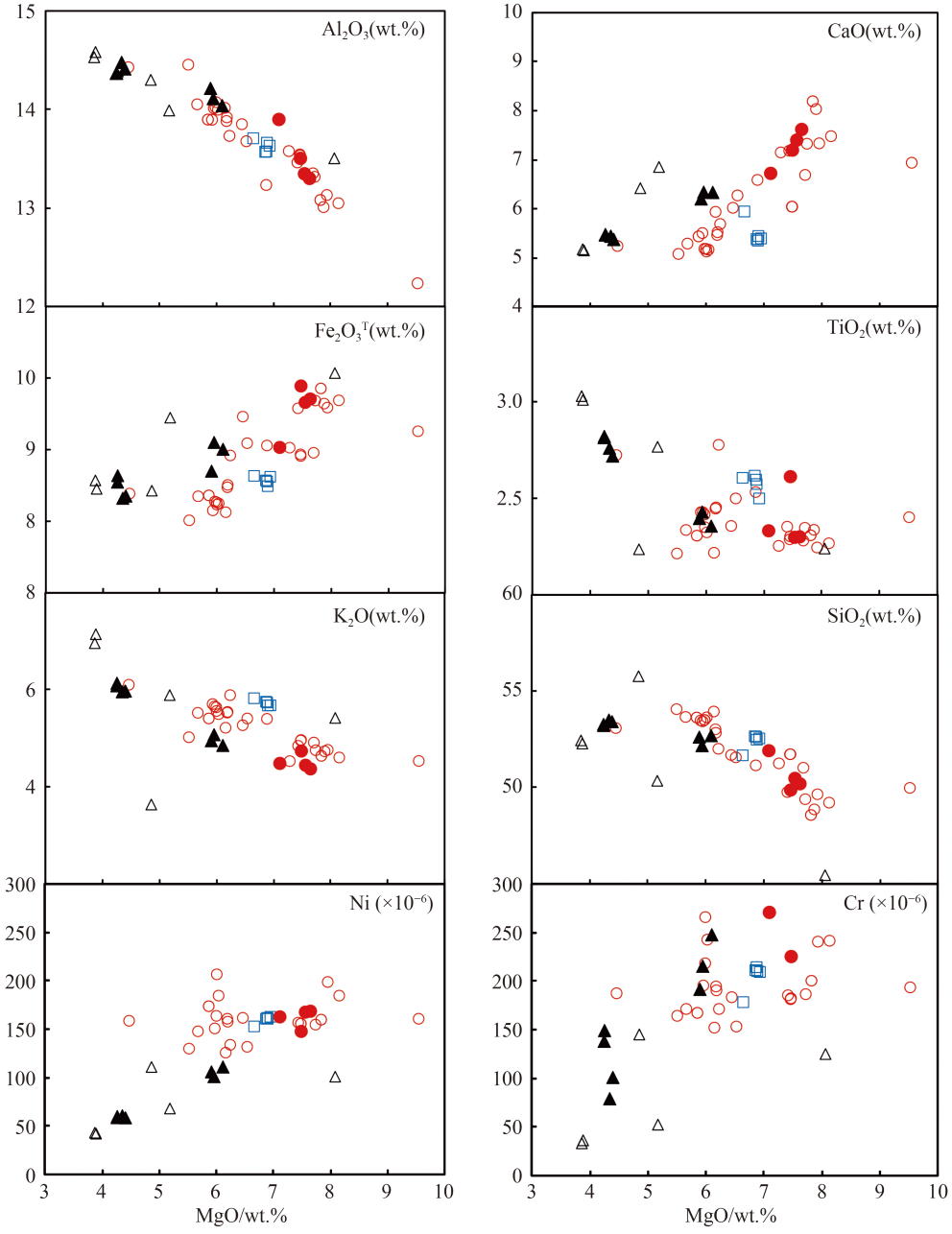

Fig. 4 Selected major and trace elements binary variation diagrams for the volcanic rocks from the Keluo and Wudalianchi volcanic districts (symbols and data source as in Fig. 3).

5.3 Sr-Nd-Pb isotopes

The Sr-Nd-Pb isotopic compositions for the rocks from the KL and WDLC volcanic districts are listed in Table 2.

The samples have high $^{87}Sr/^{86}Sr$ (0.704990–0.705272), and low $^{143}Nd/^{144}Nd$ (0.512306–0.512417). ε_{Nd} is less than 0. $^{87}Sr/^{86}Sr$ is negatively correlated with $^{143}Nd/^{144}Nd$ (Fig. 6(a) and 6(b)). Such Sr-Nd composition is remarkably different from that for primitive mantle and oceanic ridge basalt and prone to enriched mantle. The $^{206}Pb/^{204}Pb$, $^{207}Pb/^{204}Pb$, and $^{208}Pb/^{204}Pb$ ratios are about 16.546–17.135, 15.002–15.783, and 36.493–37.228, respectively, suggesting low radioactive lead content. In the $^{207}Pb/^{204}Pb$ vs. $^{206}Pb/^{204}Pb$ diagram, the rocks from the KL and WDLC volcanic districts fall in the lower left part, just above the northern hemisphere reference line (NHRL) and in the range of the EM I mantle (Fig. 6(c)). In the $^{208}Pb/^{204}Pb$ vs. $^{206}Pb/^{204}Pb$ diagram, the samples also plot above the NHRL and show good linear relationship (Fig. 6(d)). Finally, in the $^{143}Nd/^{144}Nd$ vs. $^{206}Pb/^{204}Pb$ and $^{87}Sr/^{86}Sr$ vs. $^{206}Pb/^{204}Pb$ diagrams (Figs. 6(e) and 6(f)), the investigated rocks plot close to the EM I mantle, reflecting the characteristics of enriched mantle.

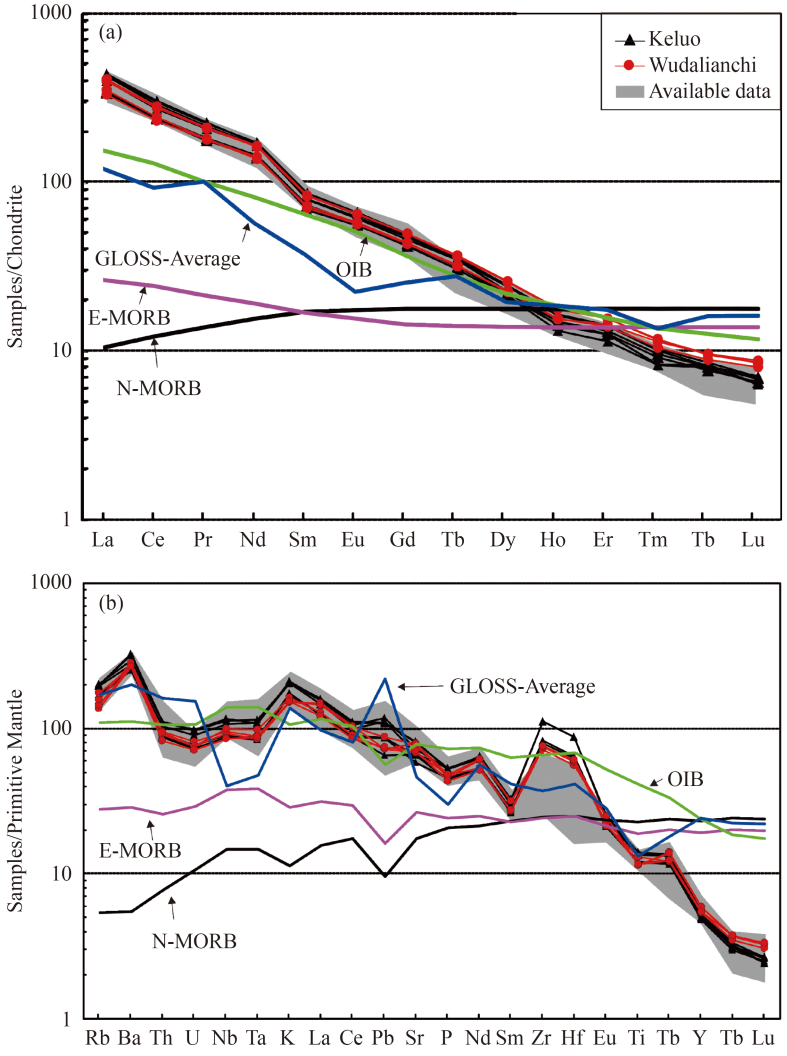

Fig. 5 (a) Chondrite-normalized (after Sun and McDonough, 1989) and (b) primitive mantle-normalized (after McDonough and Sun, 1995) multielement plots for the volcanic rocks from the Keluo and Wudalianchi volcanic districts (symbols and data source as in Fig. 3). OIB, E-MORB and N-MORB are from Sun and McDonough (1989); GLOSS-Average are from Plank and Langmuir (1998).

Table 2 Sr-Nd-Pb isotope ratios for the investigated volcanic rocks from the Keluo and Wudalianchi volcanic districts

Sample number	Wudalianchi				Keluo						
	WDLC-1	WDLC-2	WDLC-3	WDLC-4	KL-1	KL-2	KL-3	KL-4	KL-5	KL-6	KL-7
$^{87}Sr/^{86}Sr$	0.704993	0.704990	0.705060	0.705182	0.705120	0.705130	0.705177	0.705170	0.705272	0.70517	0.705139
2σ	0.000012	0.000011	0.000011	0.000017	0.000013	0.000011	0.000009	0.000014	0.000009	0.000014	0.000011
$^{143}Nd/^{144}Nd$	0.512373	0.512334	0.512417	0.512415	0.512350	0.512417	0.512412	0.512312	0.512403	0.512312	0.512306
2σ	0.000007	0.000007	0.000008	0.000011	0.000001	0.000017	0.000010	0.000008	0.000011	0.000008	0.000007
$^{206}Pb/^{204}Pb$	17.135	16.805	16.766	16.982		16.762	16.858	16.546	16.777		16.821
2σ	0.002	0.003	0.002	0.002		0.003	0.009	0.002	0.007		0.002
$^{207}Pb/^{204}Pb$	15.783	15.002	15.421	15.228		15.497	15.360	15.412	15.365		15.718
2σ	0.002	0.003	0.002	0.002		0.002	0.009	0.002	0.008		0.001
$^{208}Pb/^{204}Pb$	37.201	36.997	36.912	36.756		36.711	36.784	36.493	36.638		37.228
2σ	0.005	0.007	0.005	0.005		0.006	0.009	0.005	0.008		0.004

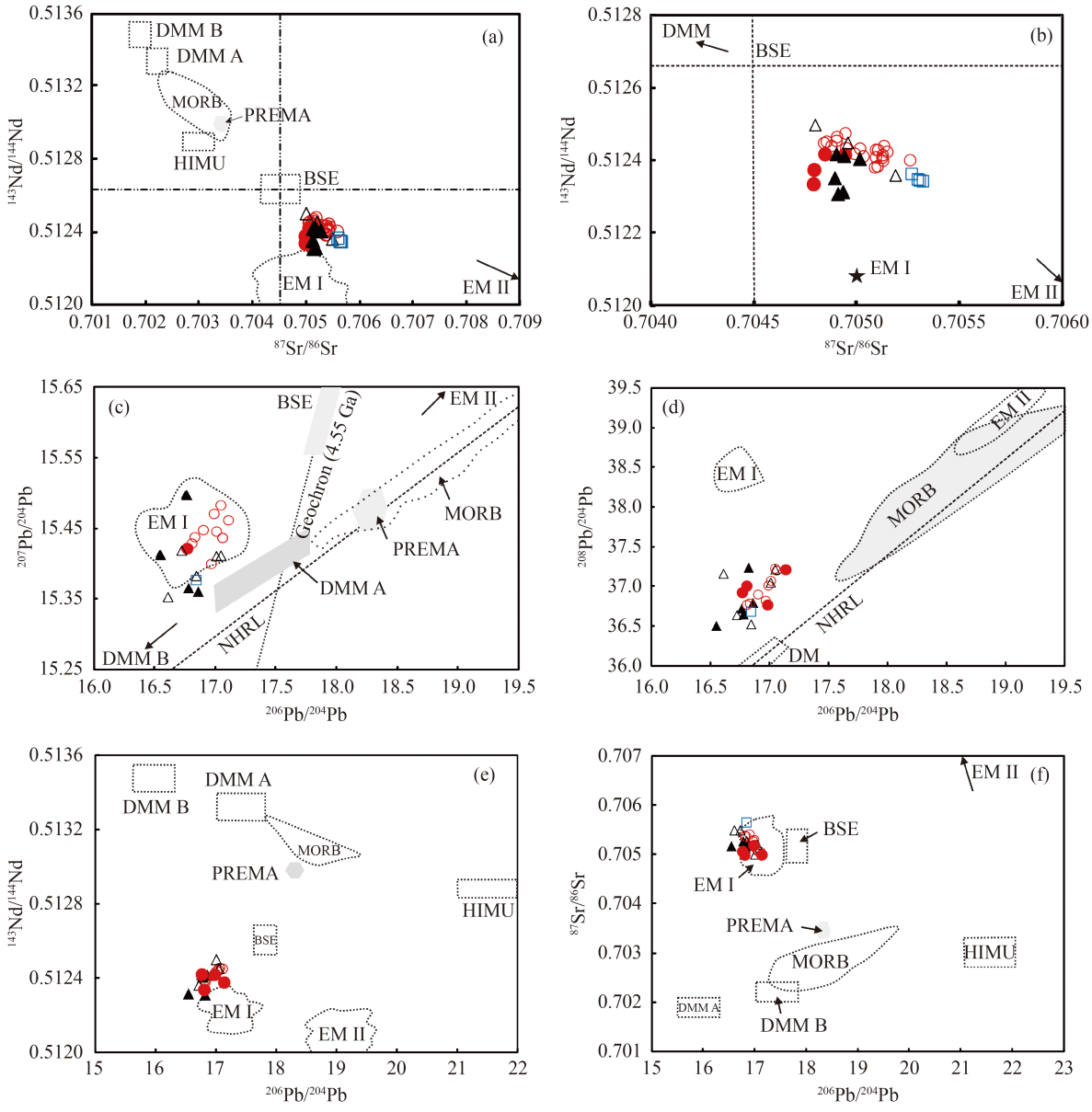

Fig. 6 (a) $^{143}Nd/^{144}Nd$ vs. $^{87}Sr/^{86}Sr$; (b) enlarged view of (a); (c) $^{207}Pb/^{204}Pb$ vs. $^{206}Pb/^{204}Pb$; (d) $^{208}Pb/^{204}Pb$ vs. $^{206}Pb/^{204}Pb$; (e) $^{143}Nd/^{144}Nd$ vs. $^{206}Pb/^{204}Pb$; (f) $^{87}Sr/^{86}Sr$ vs. $^{206}Pb/^{204}Pb$ for the volcanic rocks from the Keluo and Wudalianchi volcanic districts (symbols and data source as in Fig. 3). DMM A (depleted MORB-mantle A), DMM B (depleted MORB-mantle B), EM I (enriched mantle I), EM II (enriched mantle II), PREMA (prevalent mantle), HIMU (mantle with high $^{238}U/^{204}Pb$, U/Pb and Th/Pb values), MORB (mid-ocean ridge basalt) and BSE (bulk silicate earth) are from Zindler (1986).

6 Discussion

6.1 Crustal contamination and fractional crystallization

In theory, crustal contamination is likely to be a major process in intraplate volcanic activities as magma derived from the mantle passes through thick crust before eruption. However, the phlogopite-bearing xenoliths in the volcanic rocks from the KL and WDLC volcanic districts (Zhang et al., 2011) indicate that the magma rises too fast to be contaminated by crustal materials. Generally, the addition of crustal material to magma is expected to result in a negative covariance of $^{87}Sr/^{86}Sr$ with MgO (Carlson and Hart, 1988). The $(^{87}Sr/^{86}Sr)_i$ values of the KL and WDLC basalts vary only slightly over the range of MgO, precluding the possibility of significant crustal contamination. The $(Nb/Ta)_N$ ratios of the potassic rocks from KL and WDLC are nearly equal to 1, indicating Nb and Ta are not markedly fractionated, which shows that the potassic volcanic rocks have not suffered significant crustal contamination. Since both Nb and Ta belong to HFSE (High Field Strength Elements) and have similar geochemical behavior, the fractionation of these elements is weak in most magmatic processes (Liang et al., 2009).

In addition, the rocks contaminated by crustal materials usually have low Nb/U ratios. The Nb/U of the volcanic rocks from KL and WDLC is 38–42, similar to OIB, much higher than that of crustal rocks. It is commonly believed that Os isotopic composition is quite sensitive to crustal contamination (Xu et al., 2007; Qi and Zhou, 2008; Jung et al., 2011). The characteristics of Os isotope also suggest the volcanic rocks of WDLC experienced slight crustal contamination (with crustal contamination degree of less than 3.5%) (Chu et al., 2013). In fact, the Sr-Nd-Pb-Hf isotopes, lithophilic elements and REEs of basalts are almost not affected by such a low degree of crustal contamination (Chu et al., 2013), so they can still be used to discuss the magma source.

For the potassic rocks in the KL and WDLC districts, the MgO is relatively high, but the Ni (58×10^{-6}–169×10^{-6}) and Cr (79×10^{-6}–334×10^{-6}) contents vary significantly (Table 1), indicating the potassic magma has experienced fractional crystallization to some extent. MgO is positively correlated with Cr and Ni (Fig. 4) while the CaO/Al_2O_3 ratio decreases with MgO content, which demonstrates that the magma underwent a certain degree of olivine and clinopyroxene fractional crystallization (Fig. 7) (Liu et al., 1995). Basalt lacks obvious Eu anomaly or shows weak Eu peak and plagioclase is not visible under the microscope, indicating that magma did not undergo significant plagioclase fractional crystallization. The fractional crystallization may occur at the depth of more than 15 km (Jung and Masberg, 1998).

In summary, the characteristics of the major elements, trace elements, REEs, and Sr-Nd-Pb isotopes of the potassic volcanic rocks from the KL and WDLC volcanic districts show that magmas did not undergo intense crustal contamination or significant crystallization differentiation in shallow crust. Although fractional crystallization may occur in olivine and pyroxene, on the whole, the geochemical characteristics of the samples are still similar to that of the magma source.

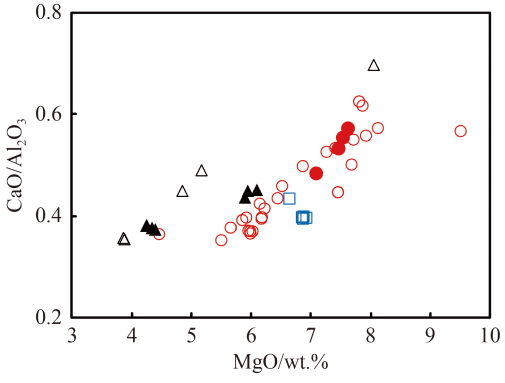

Fig. 7 CaO/Al_2O_3 vs. MgO diagram for the volcanic rocks from the Keluo and Wudalianchi volcanic districts (symbols and data source as in Fig. 3).

6.2 Source characteristic

The volcanic rocks from the KL and WDLC volcanic districts are characterized by high potassium content, low Al_2O_3 content, strong enrichment of LREEs and LILEs and particularly strong fractionation of the HREEs. The average value of $(Sm/Yb)_N$ is 9.03. The low Nd isotope ratio, low radioactive Pb isotope ratio and relatively high Sr isotopic ratio show the characteristics of EM-I-type enriched mantle. However, it is still controversial whether such mantle endmember originates from asthenosphere mantle (Xu et al., 2005; Choi et al., 2006), mantle transition zone (Kuritani et al., 2011, 2013), or continental lithospheric mantle (Fan and Hooper, 1991; Zhang et al., 1995; Zou et al., 2003; Chu et al., 2013; Duan et al., 2020).

The Nb-Ta-Ti negative anomaly in the primitive-mantle-normalized trace elements diagram for potassic volcanic rocks from the KL and WDLC volcanic districts (Fig. 5) is inconsistent with the Nb-Ta-Ti positive anomaly represented by the oceanic basalt of normal asthenosphere mantle (OIB and MORB) (Hofmann, 1986). Morever, the Ce/Pb (9.94×10^{-6}–15.96×10^{-6}) and Nb/U (37.8×10^{-6}–42.5×10^{-6}) ratio of the potassium-rich volcanic rocks are lower than that of oceanic basalt (OIB and MORB) (25 and 47) (Hofmann, 1986), indicating that it is likely a poor explanation of the petrogenesis of potassic rocks by this model.

Geophysical images have confirmed that the modern pacific plate has deeply subducted a long distance to the mantle transition zone (400–600 km) beneath the KL and WDLC districts (Zhao et al., 2011), and the potassic magma source with EM I characteristics may have originated from the mantle transition zone (Dasgupta et al., 2004; Kuritani et al., 2011, 2013). However, the magma temperature in the northern segment of Xiaoguli district near KL and WDLC is lower than that of the mantle transition zone (1250°C), while consistent with the lithosphere mantle (1180°C) (Sun et al., 2014). Consequently, it is impossible that the potassic volcanic rocks were derived from the mantle transition zone.

Crustal contamination has not played an important role in the formation of the KL and WDLC basalts. The data obtained in this study have a series of specific geochemical characteristics, including high K, LREEs, and LILEs contents, low Al_2O_3, relatively high MgO content, particularly strong HREE fractionation (with $(Sm/Yb)_N$ = 7.5−10.2), the characteristics of EM-I-type Sr-Nd-Pb isotope as well as the existence of phlogopite-bearing garnet peridotite xenoliths, which is consistent with previous studies (Zhang et al., 1995; Chu et al., 2013; Wang et al., 2017). As a result, we suggest that the volcanic rocks from the KL and WDLC volcanic districts originated from the lithospheric mantle with phlogopite-bearing garnet peridotite.

However, EM I isotope signatures suggest the existence of a mantle endmember with a time-integrated depletion

in U relative to Pb and enrichment in LREEs. The time scale required for the formation of the EM-I-type signature must be longer than 1 Ga for the SCLM (Rehkämper and Hofmann, 1997). Wang et al. (2017) estimated that it requires at least 2.2 Ga to form such a characteristic lithospheric mantle. However, During the Mesozoic and Cenozoic in east China, large-scale delamination and thinning of the lithosphere occurred (Zhu et al., 2012), and the ancient SCLM almost did not exist. Nevertheless, only when the newly formed SCLM is metasomatized can it possibly be the source of potassium-rich volcanic rocks of the KL and WDLC districts. Consequently, we propose that EM-I-type potassic rocks from the KL and WDLC volcanic districts is more likely to be derived from a new SCLM metasomated by early potassium-rich melt or fluids.

6.3 Fluid metasomatism

The existence of a potassium-rich mineral phase in the magma source is a necessary factor for the genesis of the potassic rocks from the KL and WDLC volcanic districts. Phlogopite is characterized by high K, Rb/Sr and Pb/U (Rosenbaum, 1993; Ionov and Hofmann, 1995), which is consistent with the geochemical characteristics of volcanic rocks (high $^{87}Sr/^{86}Sr$ and low $^{206}Pb/^{204}Pb$). The lherzolite xenoliths in potassic rocks from the KL and WDLC volcanic districts contain phlogopite (Zhang et al., 2011), which confirms that there is residual phlogopite in mantle beneath the study area. Currently, the focus of the debate is whether the metasomatic agents are represented by silicate melts or fluids. Some authors believe that the potassium-rich materials are silicate melts that are generated by the low-degree melting of deep asthenosphere or the delamination of lower crustal materials (Zhang et al., 2000; Zou et al., 2003; Zhang et al., 2011; Chu et al., 2013). Others argue that the potassium-rich materials come from the fluids released from ancient continental subduction sediments (Kuritani et al., 2013; Sun et al., 2015; Wang et al., 2017; Duan et al., 2019). The trace elements in volcanic rocks can be used to identify the metasomatic materials of source (Elburg and Foden, 1999; Guo et al., 2006; Guo et al., 2013; Zhang et al., 2015). When fluid metasomatism occurs, the fluids would carry a large amount of K, Rb, Ba, Sr, and Pb elements with high fluid activity but a small amount of REE, Th, and HFSE (Hf, Nb, Ta, and Zr) with low fluid activity. In contrast, when melt metasomatism occurs, melts would carry a large amount of Th, LILE, and LREE elements. Therefore, the magmatic rocks formed by fluid metasomatism often have high Ba/La, Ba/Th, Pb/U, and Sr/Th ratios, while the magmatic rocks formed by melt metasomatism have high Th/Nd, Th/U, Th/Ba, and Th/Sr ratios. The high Ba/La, Ba/Th, Pb/U, and Sr/Th ratios suggest that mantle sources of the volcanic rocks from the KL and WDLC volcanic districts were affected by fluid metasomatism (Fig. 8).

The geochemical characteristics of potassic rocks, such as high K_2O content, abnormally unradiogenic Pb isotopic compositions, and relatively low $^{87}Sr/^{86}Sr$ ratios indicate crustal materials such as metasomatic fluids. However, there is no consensus on the origin of potassium-rich fluids. The main ideas include deep asthenospheric mantle (Zhang et al., 2000), subduction zone (Elburg and Foden, 1999), delaminated SCLM (Choi et al., 2006; Zhao et al., 2014), mantle transition zone (Murphy et al., 2002; Kuritani et al., 2013) or delaminated lower continental crust (Chu et al., 2013). Kuritani et al. (2013) considered that the metasomatic fluids were derived from ancient stagnant slabs in the mantle transition zone which were released and returned to the SCLM. Recently, Wang et al. (2017) proposed the potassium-rich fluids from the mantle transition zone entered the asthenosphere, and then metasomatized the SCLM based on the study on magnesium isotopes of the potassic rocks. However, the subduction plate may have lost water when it reached the lower part of the KL and WDLC districts after a long subduction (more than 2000 km), making it impossible to provide metasomatic fluids directly (Zhang et al., 1995; Zou et al., 2003). Even if the subduction plate has carried fluids, it is difficult to release fluids under the temperature-pressure conditions of a mantle transition zone (Mibe et al., 2011). In addition, the enriched characteristics of ^{230}Th also indicate that the source of potassic rocks has not experienced the fluid metasomatism of oceanic sediments (Zou et al., 2003). Alternatively, the potassium-rich fluids are likely to be released from the delaminated ancient SCLM. The Re depletion ages (2.2−1.9 Ga) of the xenoliths in the Keluo volcano indicate that the metasomatic fluids come from the ancient SCLM (Zhang et al., 2011). Before Paleoproterozoic (> 1.9 Ga), the lithosphere mantle and lower crust in east China were dominated by granulite (Gao et al., 2003; Zheng et al., 2009; Jiang et al., 2013). The granulite is characterized by low Nd, low Pb, and high Sr isotopic ratio, which is similar to EM I mantle (Gao et al., 2004; Liu et al., 2004). The pyroxene and plagioclase minerals in lower crust granulite may contain a certain amount of water (Xia et al., 2006). With the delamination of the Mesozoic lithosphere and lower crust in east China (Gao et al., 2003; Xu et al., 2013; Meng et al., 2014), the granulite in lower crust that delaminates into asthenosphere can release a large amount of fluids. The potassium-rich fluids passed through the asthenosphere and interacted with SCLM, forming the source of potassic rocks.

6.4 Partial melting of source

In general, HREEs (e.g., Yb, Y) are relatively enriched, while LREEs (e.g., La, Ce) are relatively depleted in garnet phase. Magma evolution can be described by the characteristics of REE ratios (e.g., La/Yb, Dy/Yb) (Bogaard and Wörner, 2003). In detail, La/Yb increases

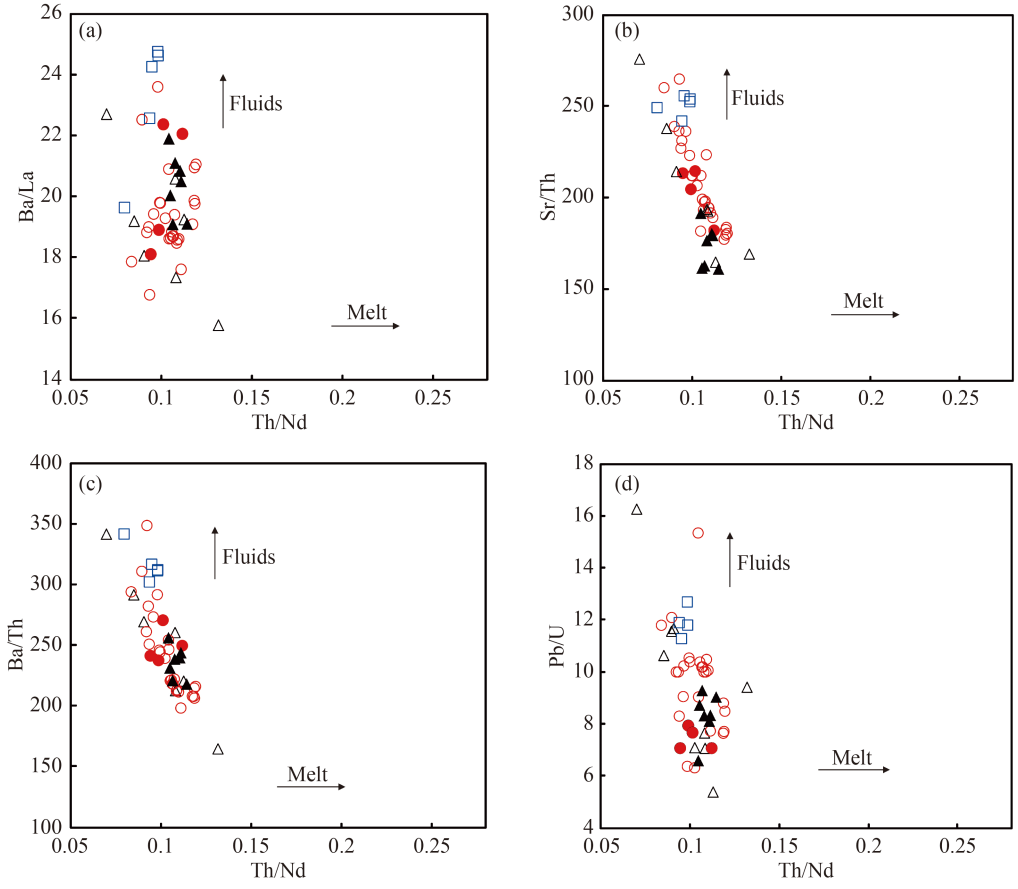

Fig. 8 (a) Ba/La, (b) Sr/Th, (c) Ba/Th and (d) Pb/U vs. Th/Nd plots for the volcanic rocks from the Keluo and Wudalianchi volcanic districts (symbols and data source as in Fig. 3). Melt and fluids metasomatism trends are indicated with arrows.

with La in partial melting processes, while La/Yb remains stable with the increase of La in a fractional crystallization process. For the volcanic rocks of KL and WDLC, La/Yb increases linearly with the increase of La (Fig. 9(a)), indicating that magmatism is mainly controlled by a partial melting process, and the fractional crystallization of olivine and clinopyroxene is only the secondary controlling factor of magma evolution. The $(Dy/Er)_N$-$(La/Sm)_N$ diagram is used to simulate the equilibrium partial melting process of potassium-rich volcanic rocks with the proportion of garnet instead of depth. It is assumed that the source consists of 15% clinopyroxene, 25% orthopyroxene, 45%−60% olivine, and 1%−15% garnet. The data of primitive mantle and the distribution coefficients are adopted from Sun and McDonough (1989) and Donnelly et al. (2004), respectively (Table 3). The simulation result indicates that garnet accounts for 2%−10% in the source of phlogopite-bearing garnet peridotite, and that potassic rocks are formed by low degree partial melting (0.5%) of the source (Fig. 9(b)).

6.5 Petrogenesis of potassic rocks

In general, the ancient lithospheric mantle of Craton wouldn't be preserved for a long time because of frequent delamination or replacement by a young lithospheric mantle during geological evolution (Griffin et al., 1999; Aulbach et al., 2004). The ancient lithospheric mantle in the lower part of North China Craton is also the same case (Gao et al., 2002; Wu et al., 2003). In Late Mesozoic, large-scale delamination and thinning of the lithosphere occurred in east China, resulting from the subduction of the Paleo-Pacific Plate. With the asthenosphere upwelled, a new SCLM formed. The fluids were released from lower crust materials that had delaminated into asthenosphere mantle at early stage. When the potassium-rich fluids rose and mixed into the new SCLM, the potassic source formed through the interaction between the new SCLM and the potassium-rich fluids.

In Cenozoic, northeast China was influenced by the subduction of Pacific Plate to East Asian continental margin, and the back-arc basin of the Japan Sea and the Northeast Asia continental rift system of the Songliao-Xialiaohe Graben were gradually formed (Liu, 1989; Ren et al., 2002). The East Asian continental rift system is composed of a group of near-parallel rifts and faults, which are distributed on both flanks of Songliao Graben with NNE-trending. From rift center (Songliao graben) to both flanks (Daxinganling and Changbai Mountains), the volcanic rocks get younger and transit from tholeiites to

Table 3 Parameters of partial melting simulation for the volcanic rocks from the Keluo and Wudalianchi volcanic districts (modified after Zhang and Guo, 2016)

	Parameters of partial melting simulation	References
Molten formula	$C_L/C_0 = 1/(D + F-DF)$	Shaw (1970)
Initial composition of the source region	PM: 0.687La, 0.444Sm, 0.737Dy, 0.480Er	Sun and McDonough (1989)
Mineral proportion of molten residual phase	0.15Cpx, 0.25Opx, 0.45−0.60Ol, 0.01−0.15Gt	Chen et al. (2007)
Partition coefficient	Cpx: 0.042La, 0.28Sm, 0.402Dy, 0.422Er;	Donnelly et al. (2004)
	Opx: 0.0005La, 0.01Sm, 0.025Dy, 0.041Er;	
	Ol: 0.00005La, 0.0006Sm, 0.004Dy, 0.0087Er;	
	Gt: 0.001La, 0.115Sm, 1.4Dy, 3.2Er	

Note: C_0—— initial content of elements, C_L—— element content in the melt, F—— Content of the melt produced during melting, D—— total distribution coefficient; PM—— primitive mantle; Cpx—— clinopyroxene, Opx—— orthopyroxene, Ol—— olivine, Gt—— garnet.

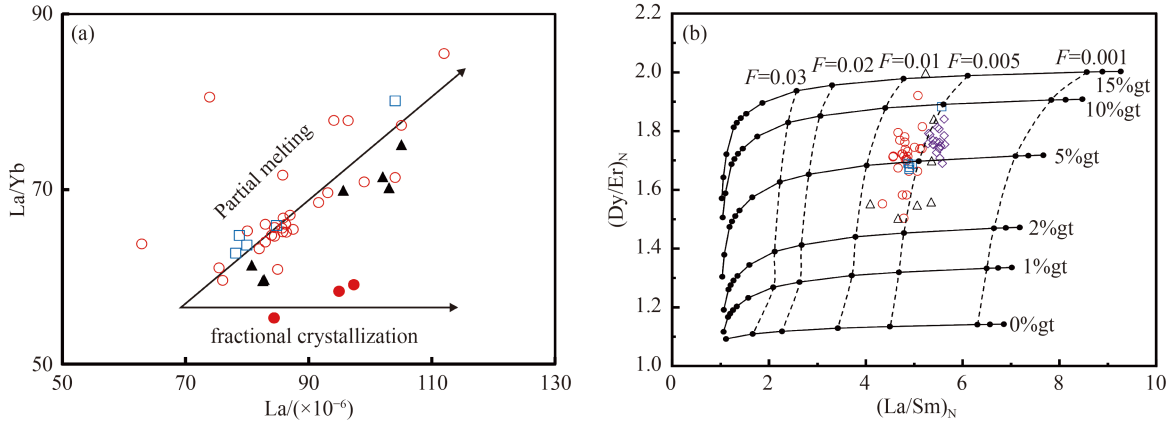

Fig. 9 (a) La/Yb vs. La and (b) $(Dy/Er)_N$ vs. $(La/Sm)_N$ diagrams for the volcanic rocks from the Keluo and Wudalianchi volcanic districts (symbols and data source as in Fig. 3). 0%gt−15%gt reflects the different proportion of garnet in the source region, F = 0.001−F = 0.03 reflects different melting degree of the source region.

alkali basalts (Liu et al., 2001). Affected by the subduction and rollback of the Pacific Plate, when the lithosphere thickness beneath the KL and WDLC districts changed dramatically, local turbulent flow occurred in the asthenosphere flow process. This promoted asthenosphere upwelling (Chen et al., 2021) and further led to lithosphere partial melting with potassic rocks formed in the KL and WDLC districts.

7 Conclusions

1) The volcanic rocks from the KL and WDLC volcanic districts are characterized by high potassium, strong enrichment of light rare earth elements (LREEs), and large ion lithophile elements (LILEs), and particularly strong fractionation of the high rare earth elements (HREEs). The high $^{87}Sr/^{86}Sr$ (0.704990–0.705272), low $^{143}Nd/^{144}Nd$ (0.512306–0.512417), and low $^{206}Pb/^{204}Pb$ (16.546–17.135) and $^{207}Pb/^{204}Pb$ (15.002–15.783) suggest that the volcanic rocks have the isotopic composition characteristics of EM-I-type mantle.

2) The potassic volcanic rocks from the Keluo and Wudalianchi volcanic districts originated from a new SCLM. The new SCLM underwent the metasomatism of potassium-rich fluids released from the lower crust material that had delaminated into asthenosphere mantle at an early stage. The potassic rocks are formed by low-degree partial melting (0.5%) of the phlogopite-bearing garnet peridotite (with garnet content of about 2%–10%).

3) In Cenozoic, affected by the subduction and rollback of the Pacific plate in northeast China, lithosphere experienced partial melting and potassic rocks formed because of asthenosphere upwelling.

Acknowledgments We are grateful to two anonymous reviewers for their constructive comments and suggestions. We sincerely thank Dr. Mu Liu at Testing Center of Institute of Geology, Ministry of Nuclear Industry in Beijing (TCIGNI) for her assistance in major, trace and isotopes analysis. This work was supported by the Marine S&T Fund of Shandong Province for Pilot National Laboratory for Marine Science and Technology (Qingdao) (No. 2021QNLM020001-1), Natural Science Foundation of Shandong Province (No. ZR2021MD083), National Natural Science Foundation of China (Grant Nos. 41302102 and 41772190), and Graduate Innovation Project of China University of Petroleum (East China) (No. YCX2021020).

References

Avanzinelli R, Elliott T, Tommasini S, Conticelli S (2007). Constraints on the genesis of potassium-rich Italian volcanic rocks from U/Th

disequilibrium. J Petrol, 49(2): 195–223

Aulbach S, Griffin W L, Pearson N J, O'Reilly S Y, Kivi K, Doyle B J (2004). Mantle formation and evolution, Slave Craton: constraints from HSE abundances and Re-Os isotope systematics of sulfide inclusions in mantle xenocrysts. Chem Geol, 208(1−4): 61–88

Bogaard P J F, Wörner G (2003). Petrogenesis of basanitic to tholeiitic volcanic rocks from the Miocene Vogelsberg, Central Germany. J Petrol, 44(3): 569–602

Carlson R W, Hart W K (1988). Flood basalt volcanism in the Northern United States. In: Macdougall J D, ed. Continental Flood Basalts. Dordrecht: Kluwer Academic Publications: 35–61

Chen Y, Ai Y S, Jiang M M, Yang Y J, Lei J S (2021). New insights into potassic intraplate volcanism in northeast China from joint tomography of ambient noise and teleseismic surface waves. J Geophys Res Solid Earth, 126(8): e2021JB021856

Chen Y, Zhang Y X, Graham D W, Su S G, Deng J F (2007). Geochemistry of Cenozoic basalts and mantle xenoliths in northeast China. Lithos, 96(1−2): 108–126

Choi S H, Mukasa S B, Kwon S T, Andronikov A V (2006). Sr, Nd, Pb and Hf isotopic compositions of late Cenozoic alkali basalts in South Korea: evidence for mixing between the two dominant asthenospheric mantle domains beneath East Asia. Chem Geol, 232(3−4): 134–151

Chu Z Y, Harvey J, Liu C Z, Guo J H, Wu F Y, Tian W, Zhang Y L, Yang Y H (2013). Source of highly potassic basalts in northeast China: evidence from Re-Os, Sr-Nd-Hf isotopes and PGE geochemistry. Chem Geol, 357: 52–66

Dasgupta R, Hirschmann M M, Withers A C (2004). Deep global cycling of carbon constrained by the solidus of anhydrous, carbonated eclogite under upper mantle conditions. Earth Planet Sci Lett, 227(1−2): 73–85

Davies G R, Stolz A J, Mahotkin I L, Nowell G M, Pearson D G (2006). Trace element and Sr-Pb-Nd-Hf isotope evidence for ancient, fluid-dominated enrichment of the source of Aldan shield lamproites. J Petrol, 47(6): 1119–1146

Donnelly K E, Goldstein S L, Langmuir C H, Spiegelman M (2004). Origin of enriched ocean ridge basalts and implications for mantle dynamics. Earth Planet Sci Lett, 226(3−4): 347–366

Duan X Z, Fan H R, Zhang H F, Yaxley G, Santosh M, Tian H C, Tan K X, Tang Z P, Xie Y S, Xiao Y L, Hou Z H, Guo H F (2019). Melt inclusions in phenocrysts track enriched upper mantle source for Cenozoic Tengchong volcanic field, Yunnan Province, SW China. Lithos, 324−325: 180−201

Duan X Z, Zhang H F, Santosh M, Tian H C, Sun H, Tan K X, Han S L, Xiao Y L, Hou Z H, Zhang Y Q, Jiang L (2020). The transformation of the lithospheric mantle beneath South China Block (SCB): constraints from petrological and geochemical studies of Daoxian and Ningyuan basalts and their melt inclusions. Int Geol Rev, 62(4): 479–502

Elburg M, Foden J (1999). Geochemical response to varying tectonic settings: an example from southern Sulawesi (Indonesia). Geochim Cosmochim Acta, 63(7−8): 1155–1172

Fan Q C, Hooper P R (1991). The Cenozoic basaltic rocks of eastern China: petrology and chemical composition. J Petrol, 32(4): 765–810

Fan Q C, Liu R X, Sui J L (1999). Petrology and geochemistry of rift type Wudalianchi K-rich volcanic rock zone. Geol Rev, 25(supp.): 358−368 (in Chinese)

Fan X L, Chen Q F, Ai Y S, Chen L, Jiang M M, Wu Q J, Guo Z (2021). Quaternary sodic and potassic intraplate volcanism in northeast China controlled by the underlying heterogeneous lithospheric structures. Geology, 49(10): 1260–1264

Foley S, Peccerillo A (1992). Potassic and ultrapotassic magmas and their origin. Lithos, 28(3−6): 181–185

Gao S, Rudnick R L, Carlson R W, McDonough W F, Liu Y S (2002). Re-Os evidence for replacement of ancient mantle lithosphere beneath the North China Craton. Earth Planet Sci Lett, 198(3−4): 307–322

Gao S, Rudnick R L, Carlson R W, McDonough W F, Liu Y S (2003). Removal of lithospheric mantle in the North China Craton: Re-Os isotopic evidence for coupled crust-mantle growth. Earth Sci Front, 10(3): 61−67 (in Chinese)

Gao S, Rudnick R L, Yuan H L, Liu X M, Liu Y S, Xu W L, Ling W L, Ayers J, Wang X C, Wang Q H (2004). Recycling lower continental crust in the North China Craton. Nature, 432(7019): 892–897

Griffin W L, Doyle B J, Ryan C G, Pearson N J, O'Reilly S Y, Davies R, Kivi K, Achterbergh E V, Natapov L M (1999). Layered mantle lithosphere in the Lac de Gras Area, Slave Craton: composition, structure and origin. J Petrol, 40(5): 705–727

Guo Z F, Wilson M, Liu J Q, Mao Q (2006). Post-collisional, potassic and ultrapotassic magmatism of the northern Tibetan Plateau: constraints on characteristics of the mantle source, geodynamic setting and uplift mechanisms. J Petrol, 47(6): 1177–1220

Guo Z F, Wilson M, Zhang M L, Cheng Z H, Zhang L H (2013). Post-collisional, K-rich mafic magmatism in south Tibet: constraints on Indian slabto-wedge transport processes and plateau uplift. Contrib Mineral Petrol, 165(6): 1311–1340

Hofmann A W (1986). Nd in Hawaiian magmas: constraints on source compositionand evolution. Chem Geol, 57(1−2): 17–30

Ionov D A, Hofmann A W (1995). Nb-Ta-rich mantle amphiboles and micas: implications for subduction-related metasomatic trace element fractionations. Earth Planet Sci Lett, 131(3−4): 341–356

Jahn B M, Wu F Y, Chen B (2000). Massive granitoid generation in central Asia: Nd isopic evidence and implication for continental growth in the Phanerozoic. Episodes, 23(2): 82–92

Jiang N, Guo J H, Chang G H (2013). Nature and evolution of the lower crust in the eastern North China Craton: a review. Earth Sci Rev, 122: 1–9

Jung S, Masberg P (1998). Major- and trace-element systematics and isotope geochemistry of Cenozoic mafic volcanic rocks from the Vogelsberg (central Germany): constraints on the origin of continental alkaline and tholeiitic basalts and their mantle sources. J Volcanol Geotherm Res, 86(1−4): 151–177

Jung S, Pfänder J A, Brauns M, Maas R (2011). Crustal contamination and mantle source characteristics in continental intra-plate volcanic rocks: Pb, Hf and Os isotopes from central European volcanic province basalts. Geochim Cosmochim Acta, 75(10): 2664–2683

Kuritani T, Kimura J I, Ohtani E, Miyamoto H, Furuyama K (2013). Transition zone origin of potassic basalts from Wudalianchi

volcano, northeast China. Lithos, 156−159: 1−12

Kuritani T, Ohtani E, Kimura J I (2011). Intensive hydration of the mantle transition zone beneath China caused by ancient slab stagnation. Nat Geosci, 4(10): 713–716

Le Bas M J, Le Maitre R W, Streckeisen A, Zanettin B (1986). A chemical classification of volcanic rocks based on the total alkali-silica diagram. J Petrol, 27(3): 745–750

Li J Y (2006). Permian geodynamic setting of northeast China and adjacent regions: closure of the Paleo-Asian Ocean and subduction of the Paleo-Pacific Plate. J Asian Earth Sci, 26(3−4): 207–224

Li N, Zhang L Y, Zhao Y W, Cao Y Y, Pan X D (2012). Genesis of potassic minerals in the Xiaoguli-Keluo-Wudalianchi-Erkeshan volcanic belt, northeast China and their geological implications. Acta Petrol Sin, 28(4): 1173−1180 (in Chinese)

Liang J L, Ding X, Sun X M, Zhang Z M, Zhang H, Sun W D (2009). Nb/Ta fractionation observed in eclogites from the Chinese Continental Scientific Drilling Project. Chem Geol, 268(1−2): 27–40

Liu C Q, Xie G H, Masuda A (1995). Geochemistry of Cenozoic basalts from eastern China—I: major element and trace element compositions: petrogenesis and characteristics of mantle source. Geochimica, 24(1): 1−19 (in Chinese)

Liu J Q (1989). Discussion on the forming and evolving of the contiental rift in the northeastern of China. Scie Geol Sin, 3: 209−216 (in Chinese)

Liu J Q (1999). Volcano in China. Beijing: Science Press (in Chinese)

Liu J Q, Han J T, Fyfe W S (2001). Cenozoic episodic volcanism and continental rifting in northeast China and possible link to Japan Sea development as revealed from K-Ar geochronology. Tectonophysics, 339(3−4): 385–401

Liu Y S, Gao S, Yuan H L, Zhou L, Liu X M, Wang X C, Hu Z C, Wang L S (2004). U-Pb zircon ages and Nd, Sr, and Pb isotopes of lower crustal xenoliths from North China Craton: insights on evolution of lower continental crust. Chem Geol, 211(1−2): 87–109

McDonough W F, Sun S S (1995). The composition of the Earth. Chem Geol, 120(3−4): 223–253

Meng F C, Safonova I, Chen S S, Rioual P (2018). Late Cenozoic intraplate basalts of the Greater Khingan Range in NE China and Khangai Province in Central Mongolia. Gondwana Res, 63: 65–84

Meng F C, Liu J Q, Cui Y, Gao J L, Liu X, Tong Y (2014). Mesozoic tectonic regimes transition in the northeast China: constraints from teporal-spatial distribution and associations of volcanic rocks. Acta Petrologica Sin, 30(12): 3569−3586 (in Chinese)

Mibe K, Kawamoto T, Matsukage K N, Fei Y, Ono S (2011). Slab melting versus slab dehydration in subduction-zone magmatism. Proc Natl Acad Sci USA, 108(20): 8177–8182

Murphy D T, Collerson K D, Kamber B S (2002). Lamproites from Gaussberg, Antarctica: possible transition zone melts of Archaean subducted sediments. J Petrol, 43(6): 981–1001

Prelevic D, Foley S (2007). Accretion of arc-oceanic lithospheric mantle in the Mediterranean: evidence from extremely high-Mg olivines and Cr-rich spinel inclusions in lamproites. Earth Planet Sci Lett, 256(1−2): 120–135

Qi L, Zhou M F (2008). Platinum-group elemental and Sr-Nd-Os isotopic geochemistry of Permian Emeishan flood basalts in Guizhou Province, SW China. Chem Geol, 248(1−2): 83–103

Rehkämper M, Hofmann A W (1997). Recycled ocean crust and sediment in Indian Ocean MORB. Earth Planet Sci Lett, 147(1−4): 93–106

Ren J Y, Tamaki K, Li S T, Zhang J X (2002). Late Mesozoic and Cenozoic rifting and its dynamic setting in eastern China and adjacent areas. Tectonophysics, 344(3−4): 175–205

Rosenbaum J M (1993). Mantle phlogopite: a significant lead repository? Chem Geol, 106(3–4): 475–483

Shaw D M (1970). Trace element fractionation during anatexis. Geochim Cosmochim Acta, 34(2): 237–243

Sun S S, McDonough W F (1989). Chemical and isotopic systematics of oceanic basalts: implications for mantle composition and processes. Geol Soc Lond Spec Publ, 42(1): 313–345

Sun Y, Ying J, Su B, Zhou X, Shao J A (2015). Contribution of crustal materials to the mantle sources of Xiaogulihe ultrapotassic volcanic rocks, northeast China: new constraints from mineral chemistry and oxygen isotopes of olivine. Chem Geol, 405: 10–18

Sun Y, Ying J, Zhou X, Shao J A, Chu Z, Su B (2014). Geochemistry of ultrapotassic volcanic rocks in Xiaogulihe NE China: implications for the role of ancient subducted sediments. Lithos, 208−209: 53−66

Tian H C, Yang W, Li S G, Ke S, Chu Z Y (2016). Origin of low δ^{26}Mg basalts with EM-I component: evidence for interaction between enriched lithosphere and carbonated asthenosphere. Geochim Cosmochim Acta, 188: 93–105

Wang X J, Chen L H, Hofmann A W, Mao F G, Liu J Q, Zhong Y, Xie L W, Yang Y H (2017). Mantle transition zone-derived EM1 component beneath NE China: geochemical evidence from Cenozoic potassic basalts. Earth Planet Sci Lett, 465: 16–28

Wu F Y, Jahn B M, Wilde S, Sun D Y (2000). Phanerozoic crustal growth: U-Pb and Sr-Nd isotopic evidence from the granites in northeast China. Tectonophysics, 328(1−2): 89–113

Wu F Y, Walker R J, Ren X W, Sun D Y, Zhou X H (2003). Osmium isotopic constraints on the age of lithospheric mantle beneath northeast China. Chem Geol, 196(1−4): 107–129

Xia Q K, Yang X Z, Deloule E, Sheng Y M, Hao Y T (2006). Water in the lower crustal granulite xenoliths from Nushan, eastern China. J Geophys Res, 111(B11): B11202

Xu J F, Suzuki K, Xu Y G, Mei H J, Li J (2007). Os, Pb, and Nd isotope geochemistry of the Permian Emeishan continental flood basalts: insights into the source of a large igneous province. Geochim Cosmochim Acta, 71(8): 2104–2119

Xu W L, Pei F P, Wang F, Meng E, Ji W Q, Yang D B, Wang W (2013). Spatial-temporal relationships of Mesozoic volcanic rocks in NE China: constraints on tectonic overprinting and transformations between multiple tectonic regimes. J Asian Earth Sci, 74(0): 167–193

Xu Y G, Ma J L, Frey F A, Feigenson M D, Liu J F (2005). Role of lithosphere–asthenosphere interaction in the genesis of Quaternary alkali and tholeiitic basalts from Datong, western North China Craton. Chem Geol, 224(4): 247–271

Xu Y G, Zhang H H, Qiu H N, Ge W C, Wu F Y (2012). Oceanic crust components in continental basalts from Shuangliao, northeast China: derived from the mantle transition zone? Chem Geol,

328(11): 168−184

Xu Y Q (1997). Eruption types and stlye of Wudalianchi volcanic belt. Heilongjiang Geo, 8(4): 3−11 (in Chinese)

Zhang M, Menzies M A, Suddaby P, Thirlwall M F (1991). EM I signature from within the post-Archaean subcontinental lithospheric mantle: Isotopic evidence from the potassic volcanic rocks in NE China. Geochem J, 25(5): 387–398

Zhang M, Suddaby P, O'Reilly S Y, Norman M, Qiu J (2000). Nature of the lithospheric mantle beneath the eastern part of the Central Asian fold belt: mantle xenolith evidence. Tectonophysics, 328(1−2): 131–156

Zhang M, Suddaby P, Thompson R N, Thirlwall M F, Menzies M A (1995). Potassic volcanic rocks in NE China: geochemical constraints on mantle source and magma genesis. J Petrol, 36(5): 1275–1303

Zhang M L, Guo Z F (2016). Origin of Late Cenozoic Abaga-Dalinuoer basalts, eastern China: implications for a mixed pyroxenite-peridotite source related with deepsubduction of the Pacificslab. Gondwana Res, 37: 130–151

Zhang M L, Guo Z F, Cheng Z H, Zhang L H, Liu J Q (2015). Late Cenozoic intraplate volcanism in Changbai volcanic field, on the border of China and North Korea: insights into deep subduction of the Pacific slab and intraplate volcanism. J Geol Soc London, 172(5): 648–663

Zhang X Z, Yang B J, Wu F Y, Liu G X (2006). The lithosphere structure in the Hingmong-Jihei (Hinggan-Mongolia-Jilin-Heilongjiang) region, northeast China. Geo China, 33(4): 816−823 (in Chinese)

Zhang Y L, Liu C Z, Ge W C, Wu F Y, Chu Z Y (2011). Ancient sub-continental lithospheric mantle (SCLM) beneath the eastern part of the Central Asian Orogenic Belt (CAOB): implications for crust-mantle decoupling. Lithos, 126(3−4): 233–247

Zhao D P, Yu S, Ohtani E (2011). East Asia: seismotectonics, magmatism and mantle dynamics. J Asian Earth Sci, 40(3): 689–709

Zhao Y, Yang Z Y, Ma X H (1994). Geotectonic transition from paleoasian system and paleotethyan system to paleopacific active contiental margin in eastern Asia. Sci Geol Sin, 29: 105−119 (in Chinese)

Zhao Y W, Li N, Fan Q C, Zou H B, Xu Y G (2014). Two episodes of volcanism in the Wudalianchi volcanic belt, NE China: evidence for tectonic controls on volcanic activities. J Volcanol Geotherm Res, 285: 170–179

Zheng J P, Griffin W L, O'Reilly S Y, Zhao J H, Wu Y B, Liu G L, Pearson N, Zhang M, Ma C Q, Zhang Z H, Yu C M, Su Y P, Tang H Y (2009). Neoarchean (2.7–2.8 Ga) accretion beneath the North China Craton: U-Pb age, trace elements and Hf isotopes of zircons in diamondiferous kimberlites. Lithos, 112(3−4): 188–202

Zhou J B, Wilde S A, Zhang X Z, Zhao G C, Zheng C Q, Wang Y J, Zhang X H (2009). The onset of Pacific margin accretion in NE China: evidence from the Heilongjiang high-pressure metamorphic belt. Tectonophysics, 478(3−4): 230–246

Zhu R X, Yang J H, Wu F Y (2012). Timing of destruction of the North China Craton. Lithos, 149: 51–60

Zindler A, Hart S R (1986). Chemical geodynamics. In: Workshop on the Earth as a Planet, 14: 493–571

Zou H B, Reid M R, Liu Y S, Yao Y P, Xu X S, Fan Q C (2003). Constraints on the origin of historic potassic basalts from northeast China by U-Th disequilibrium data. Chem Geol, 200(1−2): 189–201